

COMPARISON OF ANISOTROPIC AND INERTIAL EFFECTS IN SINGLE CRYSTALS UNDER MICROSCALE LASER SHOCK PEENING

Siniša Vukelić, Jeffrey W. Kysar, and Y. Lawrence Yao
Mechanical Engineering Department
Columbia University
New York, NY

KEYWORDS

Laser, Microscale, Shock Peening, Anisotropy

ABSTRACT

The process of laser shock peening induces compressive residual stresses in a material to improve material fatigue life. For micron-sized laser beams, the size of the laser-target interaction zone is of the same order of magnitude as the target material grains and thus the target material must be considered as being anisotropic and inhomogeneous. Single crystals are chosen to study the effects of the anisotropic mechanical properties. In the present study, numerical and experimental aspects of laser shock peening on (110) crystal surface, of aluminum single crystals are studied. Two numerical models have been developed, one that takes into account solely anisotropy as well as one that also includes inertial terms to predict size and nature of the deformation and residual stresses. Results of both models were compared among each other and against experimental findings for validation purposes.

INTRODUCTION

Laser shock peening (LSP) is a surface treatment that improves fatigue life and wear

resistance of the treated parts. In this process, laser-induced shocks induce compressive residual stresses into the target material with no thermally induced microstructure change (Clauer and Holbrook 1981; Hammersley et al. 2000). The treatment is similar to the conventional shot peening, but induced residual stresses penetrate much deeper into the target material. However, the high cost of the high-powered lasers required for the treatment of large areas has prevented wider industrial application of LSP.

The recent development of various microdevices (e.g., MEMS, microswitches, etc.) has raised the possibility of improved reliability of system components by using microscale LSP (μ LSP). Much work in this field has been performed on polycrystalline materials (Zhang and Yao 2000). However, in μ LSP the beam spot size is several microns and the average grain size in polycrystalline aluminum and copper is about same order of magnitude, which means that in most cases only a few grains at most are affected by a single laser pulse. Therefore, the material properties must be considered as anisotropic and heterogeneous.

This has motivated a prior study of the response of single crystals of aluminum and copper subjected to laser shock processing in order to better understand the effects of anisotropy (Chen et al. 2004). A quasi-static

numerical model was established and the results compared to experiments for two different orientations of aluminum and copper single crystals. Albeit neglecting inertial terms in the governing equations represents a gross simplification of highly dynamic process, it gave some insight of single-crystal response to the Gaussian pressure loading.

Further research on the effects of anisotropy under μ LSP was analytical through utilization of the anisotropic slipline theory developed by Hill (1950) and generalized by Rice (1973). Wang et al. (2008) estimated the size of the deformed region due to laser shock peening on an aluminum single crystal of a nonsymmetric (114) orientation assuming a Gaussian pressure distribution from the laser shock. The approximate analytical solution has been augmented with a finite element numerical analysis that did not account for inertial effects and work hardening. The comparison between the two has shown good agreement. A symmetric orientation of (110), which activates multiple slip systems, was investigated by Vukelić et al. (2008) and was compared with the (114) case.

Shock-wave propagation in isotropic materials under LSP has been studied by Peyre et al. (2003) and Fan et al. (2005). This work sheds light on the shock-wave propagation and subsequent material response, not including effects of anisotropy. Single-crystal plasticity was combined with dynamic loading by Nemat-Nasser et al. (1998) to study dynamic void collapse. Vukelić et al. (2008) included effects of inertia as well as work hardening to examine single-crystal anisotropic material response to μ LSP.

The objective of this work is to study aluminum single-crystal behavior under Gaussian pressure distribution induced by μ LSP, and to compare the relative effects of anisotropy and anisotropy combined with inertia. Further, the influence of these two competing effects in the overall deformation process will be investigated.

EXPERIMENTAL SETUP

An aluminum single crystal with (110) orientation is used in this study. The sample is mounted on a three-circle goniometer and its orientation is determined by Laue diffraction. The specimen is cut to size with a wire electrical

discharge machine (EDM), and the resulting heat-affected zone (HAZ) is removed via mechanical polishing. Finally, electropolishing is used to remove any residually deformed material. Laser shock peening is then applied along a line on the specimen surface. The shocked surface is then characterized with various methods, after which the crystal is sectioned with wire EDM and the cross section surface is again mechanically polished and electropolished to examine the plastic deformation that occurs on the cross section.

A frequency-tripled Q-switched Nd:YAG laser with wavelength $\lambda = 355$ nm in TEM₀₀ mode is used for the μ LSP experiments with a beam diameter of 12 μ m, pulse duration of 50 ns, and laser intensity of about 4 GW/cm². A 16 μ m thick polycrystalline aluminum foil is used as an ablative coating applied tightly over an evenly spread layer (10 μ m thick) of high-vacuum grease. The specimen shown in Figure 1 is put into a shallow container filled with distilled water. To obtain an approximate 2-D deformation state, shocks are applied with a 25- μ m spacing along the (110) direction. Detailed discussion about formation of the approximate two-dimensional deformation can be found in Rice (1987).

μ LSP induces rotation of the crystal lattice as a consequence of plastic deformation in the single crystal, which can be characterized experimentally by comparing the as-deformed crystallographic orientation (Kysar and Briant 2002) to the known undeformed state. Lattice orientation is measured using electron backscatter diffraction (EBSD) with micrometer-scale spatial resolution. For these measurements, an HKL Technology system attached to a JEOL JSM 5600LV scanning electron microscope (SEM) is used to scan the shocked surface and cross section, respectively.

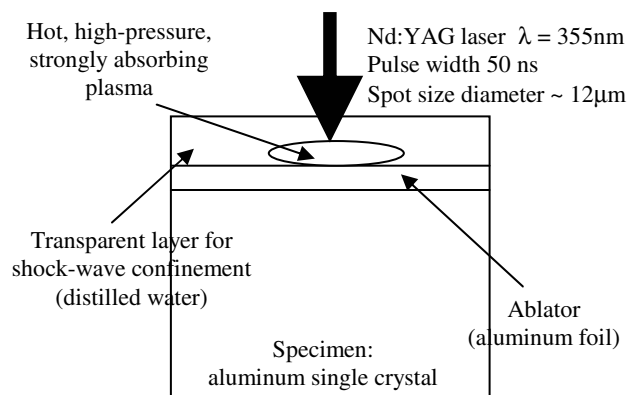


FIGURE 1. EXPERIMENTAL SETUP.

X-ray microdiffraction is used to characterize the residual stress near the shock line. Synchrotron radiation as a source of X-ray beams is employed. The beam is focused using a glass capillary such that a spatial resolution of several microns can be achieved. Beamline X20A at the National Synchrotron Light Source at Brookhaven National Laboratory (NSLS) is used for the diffraction measurements with monochromatic synchrotron radiation at 8.0 KeV. Measurements are conducted along a line perpendicular to the shock line with 10- μm spacing. The measured X-ray profile is processed using Ungar's method (1983).

NUMERICAL MODELING

Problem Formulation

The analysis is performed with the commercial finite element program ABAQUS/Standard with a User Defined Material subroutine (UMAT), based on single-crystal plasticity theory formulated by Asaro (1983), written by Huang (1991) and modified by Kysar (1997). For the purpose of this analysis, the crystallographic orientation relative to the finite element mesh is chosen such that plane strain is achieved (Chen et al. 2004). Pressure is applied on the (110) surface. Two simulations have been performed. The first assumes quasi-static conditions, which gives insight into the role of the anisotropy, especially in comparison to the analytical solution (Wang et al. 2008; Vukelić et al. 2008). The peak pressure is taken to be $P_o = 2200$ MPa and treated as semi-free parameter to match experimental results of displacement. Boundary conditions are specified as follows: zero traction on the side edges; zero vertical displacement on the bottom. In addition to anisotropy, in the second simulation, the dynamic aspect of μLSP process is added by taking into account inertia. For this case, boundaries are modeled with semi-infinite elements, and therefore there are no reflections of the elastic waves once they propagate through the domain of interest. In both simulations, the initial yield stress is set to be 300 MPa and saturation stress 600 MPa, values that appear to be reasonable, following Nemat-Nasser et al. (1998) and Peyre et al. (2003).

The loading for both the quasi-static and dynamic cases is Gaussian spatial distribution pressure:

$$P(x) = P_o \exp\left(-\frac{x^2}{2R^2}\right) \quad (1)$$

However, in the case when the effects of inertia are considered, a temporal aspect is added to the pressure. Peyre et al. (2003) measured the temporal pressure profile of pulses with 3 ns and 10 ns duration using VISAR technique. They reported that as the duration of laser pulse increases, the peak pressure value decreases and full-width-at-half-maximum (FWHM) increases. Following this formulation, the temporal profile is generated as a semi-free parameter to match the experimental findings of displacement and lattice rotation. The temporal pressure profile is shown in Figure 2. In addition, to accommodate lateral growth of plasma, the radius is set to be three times larger than the radius of the laser spot.

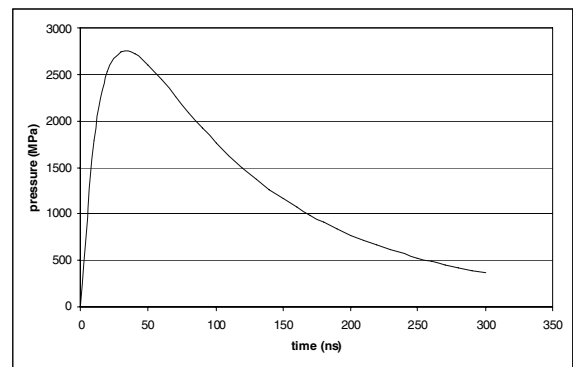


FIGURE 2. TEMPORAL PRESSURE DISTRIBUTION DURING LOADING IN DYNAMIC NUMERICAL SIMULATION.

Constitutive Relationships

The dynamic loading and wave propagation are characterized using a formulation based on the dynamic principle of virtual work. Equilibrium equations are employed in the quasi-static case. At the end of each solution increment, the main program passes the UMAT the following variables: time increment, stress state, strain increment, and solution-dependent state variables ($s_i^{(\alpha)}, n_i^{(\alpha)}, \gamma^{(\alpha)}, g^{(\alpha)}$, etc.) defined by the user. The UMAT updates the stress state and solution-dependent variables and calculates the material Jacobian matrix $\partial\sigma_{ij}/\partial\varepsilon_{kl}$ based on the equations below. These new values are then returned to the solver where the new stress state is applied as a load increment and then the corresponding strain increment is calculated.

This process is repeated until the job is complete.

When loading of an elastic-plastic crystal takes place, total strain rate is given as a sum of its elastic and plastic components, assuming an infinitesimal deformation gradient tensor:

$$\dot{\boldsymbol{\varepsilon}}_{ij} = \dot{\boldsymbol{\varepsilon}}^e + \dot{\boldsymbol{\varepsilon}}^p \quad (2)$$

The FEM analysis accounted rigorously for the finite deformation kinematic. However, for simplicity, we discuss here the small-strain version of the theory to highlight the salient points. According to Schmid (1931), plastic slip occurs when the shear stress resolved on the crystallographic plane in the slip direction reaches some critical value. The Schmid factor is defined as:

$$\mu_{ij}^{(\alpha)} = \frac{1}{2} (s_i^{(\alpha)} n_j^{(\alpha)} + s_j^{(\alpha)} n_i^{(\alpha)}) \quad (3)$$

where $s_i^{(\alpha)}$ and $n_i^{(\alpha)}$ are vectors that define slip directions and slip normals on the α -th slip system, respectively. The Schmid factor is used to calculate the resolved shear stress $\tau^{(\alpha)}$ and plastic strain rate on each particular slip system:

$$\tau^{(\alpha)} = \sigma_{ij} \mu_{ij}^{(\alpha)} \quad (4)$$

$$\dot{\boldsymbol{\varepsilon}}_{ij}^p = \sum_{\alpha=1}^N \mu_{ij}^{(\alpha)} \dot{\gamma}^{(\alpha)} \quad (5)$$

where σ_{ij} is stress tensor, $\dot{\gamma}^{(\alpha)}$ is engineering shear strain rate on the α -th slip system, and summation is done over all N slip systems.

The magnitude of the plastic strain increment is determined using the rate-dependent power-law formulation introduced by Hutchinson (1976):

$$\dot{\gamma}^{(\alpha)} = \gamma_0^{(\alpha)} \operatorname{sgn}(\tau^{(\alpha)}) \left| \frac{\tau^{(\alpha)}}{g^{(\alpha)}} \right|^m \quad (6)$$

where $\gamma_0^{(\alpha)}$ is reference shear strain rate and $g^{(\alpha)}$ is the strength of the α -th slip system. With this formulation, significant slip occurs only on those systems for which $\tau^{(\alpha)} \cong g^{(\alpha)}$.

Hardening of the material is characterized through evolution of the strength, $g^{(\alpha)}$, of each slip system. With increasing plastic deformation,

$g^{(\alpha)}$ evolves as a function of hardening moduli $h_{\alpha\beta}$, which can be decomposed into self-hardening ($\alpha = \beta$) and latent-hardening ($\alpha \neq \beta$) moduli, and shear strain rate.

$$g^{(\alpha)} = \sum_{\beta=1}^N h_{\alpha\beta} \dot{\gamma}^{(\beta)} \quad (7)$$

In this study, the Pierce, Asaro, and Needleman (1983) model is used to simulate hardening.

$$h_{\alpha\alpha} = h(\gamma) = h_0 \sec h^2 \left| \frac{h_0 \gamma}{\tau_s - \tau_0} \right| \quad (8)$$

$$h_{\alpha\beta} = qh(\gamma), (\alpha \neq \beta) \quad (9)$$

where h_0 is initial hardening modulus, τ_0 is initial value of resolved stress, τ_s is saturation stress of hardening moduli and q is ratio between latent-hardening rate and self-hardening rate of a particular slip system.

The stress rate associated with the elastic strain rate can be formulated as:

$$\dot{\boldsymbol{\sigma}}_{ij} = L_{ijkl} \dot{\boldsymbol{\varepsilon}}_{kl} = L_{ijkl} \left(\dot{\boldsymbol{\varepsilon}}_{kl}^e - \dot{\boldsymbol{\varepsilon}}_{kl}^p \right) \quad (10)$$

where L_{ijkl} is elastic moduli tensor.

RESULTS AND DISCUSSION

Deformation Measurements and Comparison with Simulation Results

Deformation measured via a Keyence optical profilometer superimposed with numerical results for comparison is shown in Figure 3. Measurements are taken at several different locations along the shocked line, and deformations appear to be quite uniform. Both quasi-static and dynamic models capture the trend of the deformation well. However, both quasi-static and dynamic models underestimate the maximum value of deformation by about 40% and 20%, respectively. Also it should be noted that the quasi-static model predicts the pileup of the material observed in the experiments. Pileup is a consequence of the plastic deformation wherein the material underneath the high pressure is deformed downward, and on both sides the material is piled-up, i.e., deformed piled-up. The difference in response comes from the nature of the

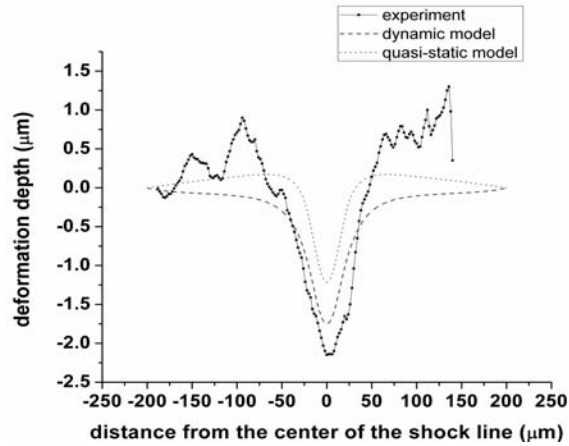


FIGURE 3. DEFORMATION FIELD MEASURED VIA PROFILOMETER AND COMPARED WITH NUMERICAL RESULTS.

pressure load. In the dynamic case, load is applied as a very short impulse and it propagates as a wave into the depth of the material, plastically deforming it, whereas when the inertial terms are neglected, the specimen is subject to the punch-like loading, i.e., a distributed loading over a finite region of the surface, which induces the material pileup to the left and right of the punch.

Lattice Rotation Measurements via EBSD and Comparison with Simulation Results

Chen et al. (2004) and Wang et al. (2008) demonstrated experimentally that plastic deformation due to μ LSP will cause rotation of the crystallographic lattice, which can be characterized by means of electron backscatter diffraction (EBSD) measurements of the attendant lattice rotation. Experimental results shown here are reported elsewhere (Vukelić et al. 2008) and are used for validation purposes.

Experimental results for the lattice rotation fields on the top surface and in the cross section are shown in Figures 4a and 4b, respectively. Rotation about the shock line center is antisymmetric, the blue region corresponding to counterclockwise rotation (CCW) and the red region corresponding to clockwise rotation (CW). Deformation is largely uniform along the shock line on the treated surface, which indicates that an approximate two-dimensional deformation state is achieved by shocking the single crystal along the (110) direction. The magnitude of lattice rotation is largest between $\pm 55 \mu\text{m}$ from the center of shock line and it is different for the

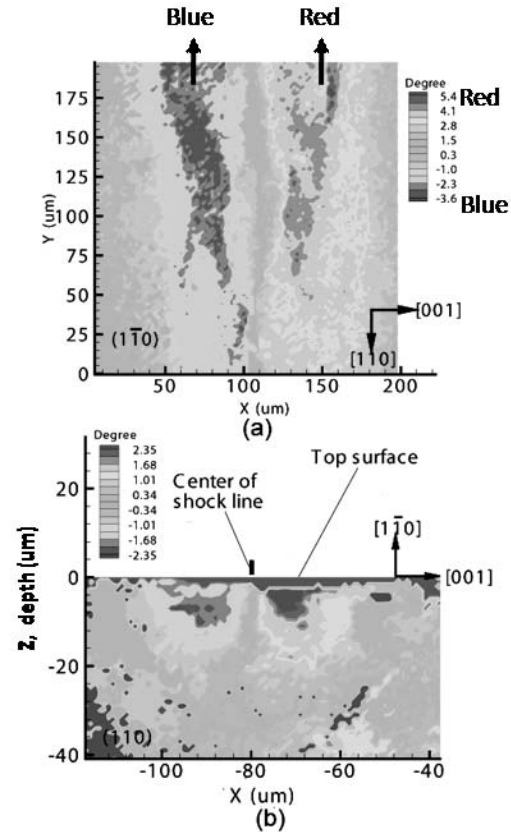


FIGURE 4. LATTICE ROTATION CONTOUR MAP: (a) SAMPLE SURFACE, (b) (110) CROSS SECTION.

two cases: it is between $\pm 4^\circ$. Similar lattice rotation results, in terms of magnitude, are seen in EBSD measurement on the cross section (Figure 4b). Here the lattice rotates between $\pm 2.4^\circ$.

In Figure 5, the FEM simulation of in-plane lattice rotation for the dynamic and quasi-static cases is shown. Both simulations show similar trends and are in good agreement with experimental findings. However, a few important differences should be noted. The quasi-static case predicts larger maximum values of the lattice rotation and overestimates it in comparison to the experiments. It also penetrates less into the sample depth. The reason for this is that, in the case when inertial terms are ignored, the material is subject to long-lasting surface traction of constant magnitude with time, and deformation is concentrated closer to the top surface, resulting in shallower deformation that is higher in magnitude. On the other hand, the dynamic case initiates waves that propagate through the target material and cause plastic deformation that is therefore deeper and smaller in magnitude.

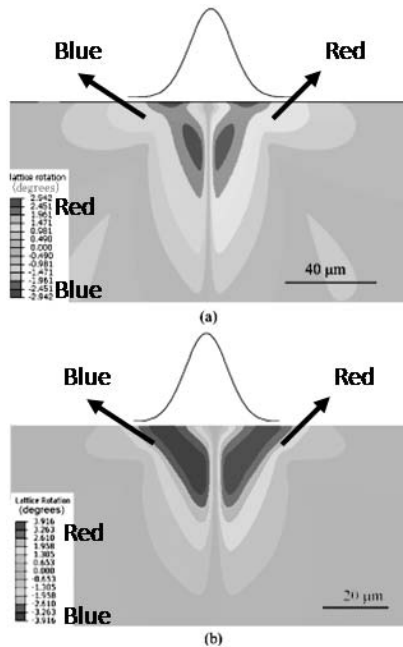


FIGURE 5. LATTICE ROTATION BY FEM: (a) DYNAMIC MODEL, (b) QUASI-STATIC MODEL.

Stress Distribution

The residual stresses were characterized experimentally based on microdiffraction experiments and analyzed using a method proposed by Ungar (1983) that assumes that the deformed crystal is composed of cell walls and soft cell interiors. When pressure loading is applied to such a composite model, the cell walls are under compression and cell interiors experience tensile stress. Thus, an asymmetric diffraction peak can be decomposed into two symmetric peaks that belong to 'walls' and 'interiors' shifted to the left and right from the undeformed diffraction peak, respectively. Measuring the relative difference in angle with respect to the reference undistorted profile will lead to a relative change of lattice spacing, Δd , which allows one to estimate the variation in the stress state, $\Delta\sigma$, induced by the plastic deformation.

Experimentally, the diffraction profile is measured along a line perpendicular to the shock line with 10 μm between each measurement. Weighted averages of the residual stresses from the numerical simulations are superimposed to Figure 6. A weight function is chosen that takes into account the fractional contribution of progressively deeper layers to the diffracted intensity (Vukelić et al. 2008b). The

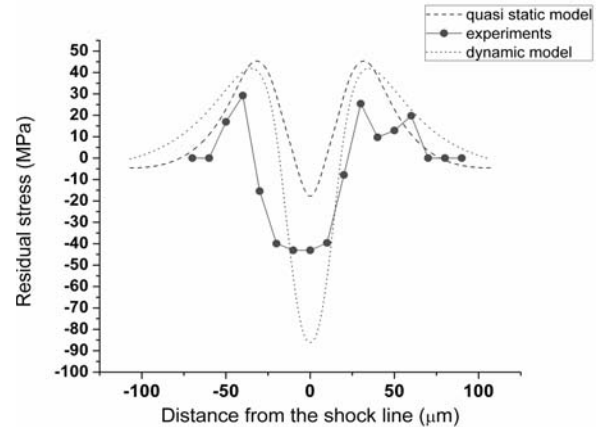


FIGURE 6. RESIDUAL STRESS DISTRIBUTION IN 1-1 DIRECTION.

dynamic model agrees with the experimental findings very well, predicting large compressive residual stress in the middle with self-equilibrating tensile regions on the left-end right side of the field whereas quasi-static loading predicts residual stress in the 1-1 direction to be predominantly tensile.

Shear Strain Increments

Plastic deformation in the simulation is represented through shear strains. It is of interest to closely examine shear strain increments for each slip system as well as the total shear strain increment. These are shown on Figures 7a and 7b for both the dynamic and quasi-static loading cases. From Figure 7, it can be seen that for both cases shear increments associated with slips *i* and *iii* are antisymmetric with respect to the center line of the Gaussian pressure distribution, whereas the shear increment on slip system *ii* is symmetric.

For plane strain conditions, only six slip systems out of a total of 12 in face-centered cubic (FCC) crystals remain active (Rice 1987), which form three effective slip systems. When quasi-static pressure loading is applied to the (110) surface, according to the analytical solution based on the anisotropic slipline theory the entire deformation field is divided into sectors. In each of those sectors, one or two slips systems are active. Boundaries of sectors are slip directions and slip normals, which represent lines of stress discontinuity (Rice 1987). Approximating μLSP as a punch problem with nonuniform pressure loading, the deformation field can be constructed through employment of the concepts of Rice (1987). The analytical solution agrees well with

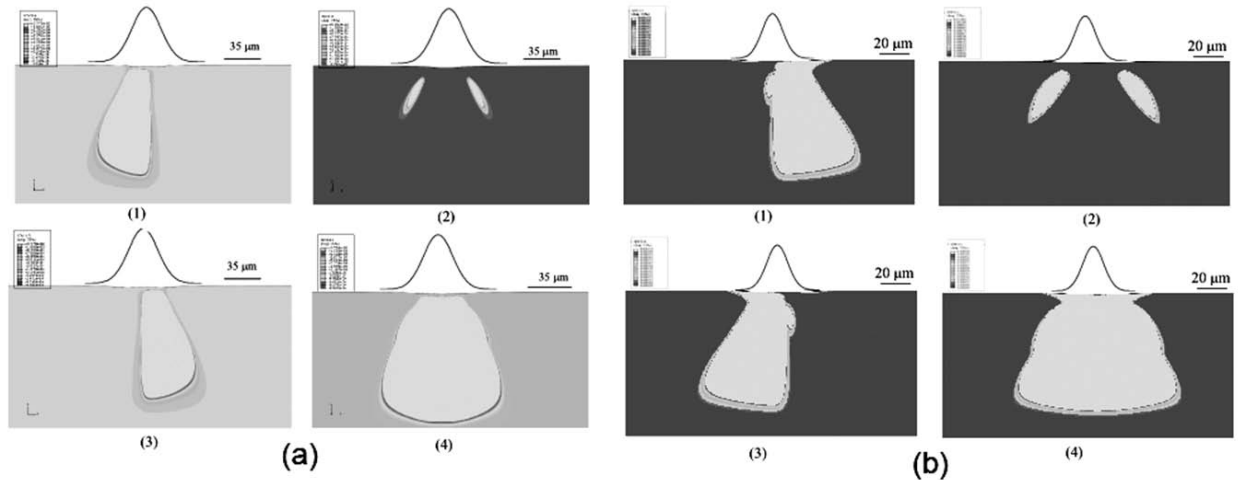


FIGURE 7. PLASTIC SHEAR IN EACH SLIP SYSTEM AT THE END OF THE LOADING STEP. GRAY AREA REPRESENTS LOCATION AT WHICH SHEAR EXCEEDED 10^{-3} s^{-1} . (a) DYNAMIC MODEL, (b) QUASI-STATIC MODEL. (1) INCREMENT IN SLIP SYSTEM *i*, (2) INCREMENT IN SLIP SYSTEM *ii*, (3) INCREMENT IN SLIP SYSTEM *iii*, (4) TOTAL SHEAR STRAIN INCREMENT.

the finite element analysis in the case of the ideally plastic material (Wang 2008; Vukelić et al. 2008). When strain hardening is taken into account, the results deviate from the previous studies. Shear strains on slip systems *i* and *iii* are activated only in the triangle below the punch loading and penetrate deeper into the material. A remnant of the analytical solution can be observed in total shear increment as well as on shear increments on slip systems *i* and *iii* (Figure 7b, 1, 2, and 4). The upper edge of the plastically deformed material has an angle of 35.3° corresponding to slip systems *i* and *iii* and forms a central triangular region under the load.

Propagation of the elastic precursor wave that precedes plastic deformation under μLSP process, seen in the case when dynamic loading is applied, is analogous to the elastic propagation of waves, used in nondestructive evaluation (NDE) for calculation of ultrasonic field profiles in mildly anisotropic media. This approach considers wave propagation from a finite-sized transducer source, which is analogous to the compressive surface traction induced by Gaussian pressure distribution. The basis for the NDE is Huygen's principle and retarded potentials based on the existence and properties of the temporal Fourier transformation of Green's function. Tverdokhlebov and Rose (1988), employing the Helmholtz decomposition, represented Green's function as a sum of three components corresponding to plane wave propagation of quasi-longitudinal and two quasi-

transverse velocities present in the arbitrary anisotropic, homogeneous solid. Furthermore, they obtained the solution for the point-source problem considering first-order weak anisotropy approximation. Numerical implementation is done by Rose et al. (1989). Results are obtained for centrifugally cast stainless steel (CCSS) compared with experimental findings of Kupperman et al. (1987).

Numerical integration of Green's function presented by Rose et al. (1989) as an output gives elastic wave velocity profiles. These transducer field profiles in essence represent strain energy density, and from them it can clearly be seen that deformation propagates in the direction of the applied load with little lateral expansion beyond the boundaries of the source. In the case of μLSP , this effect is observed through examination of total shear increments, discussed in the previous paragraph. In addition, another important consequence of anisotropy should be noted; the direction of the wavefront normal vector does not coincide with the wave velocity vector for an anisotropic medium. This leads to skewing of the direction of the strain energy density propagation in the direction of large phase velocity, resulting in asymmetric material response.

CONCLUSION

A comparison between effects of anisotropy and anisotropy coupled with inertia in single-crystal aluminum under microscale laser shock

peening is presented. A preexisting quasi-static model has been extended to take into account work hardening and lateral plasma expansion. The trend in displacement and crystallographic lattice rotation is captured well by both models. The residual stress prediction of the quasi-static model does not match experimental findings, whereas the dynamic one shows good agreement. Plastic deformation is observed through shear strain increments. When strain hardening is taken into account without inertial effects, the numerically predicted deformation field deviates from the analytical solution significantly. The dynamic case shows that deformation propagation is analogous to wave propagation studied in nondestructive material evaluation.

ACKNOWLEDGMENT

This work is supported by NSF grant DMI 0500239. Help provided by Dr. Jean Jordan Sweet of IBM Watson Research Center with the use of X-ray microdiffraction equipment at the National Synchrotron Light Source at Brookhaven National Laboratory is greatly appreciated. This work has used the shared experimental facilities that are supported primarily by the MRSEC program of NSF under award number DMR 0213574 by the New York State Office of Science, Technology and Academic Research (NYSTAR). Panjawat Kongsuwan helped with formatting the paper.

REFERENCES

Asaro RJ (1983). Micromechanics of crystals and polycrystals. *Adv. in Appl. Mechanics*, 23, pp1-115.

Chen HQ, JW Kysar, YL Yao (2004). Characterization of plastic deformation induced by microscale laser shock peening. *J. of Appl. Mech.*, 71(5), pp713-723.

Clauer AH, JH Holbrook (1981). Effects of laser induced shock waves on metals. *Shock waves and high strain phenomena in metals – Concepts and applications*. New York, pp675-702.

Fan Y, Y Wang, S Vukelić, YL Yao (2005). Wave-solid interactions in laser-shock-induced deformation processes. *J. of Appl. Physics*, 98(10), pp104904-104904-11.

Hammersley G, LA Hackel, F Harris (2000). Surface prestressing to improve fatigue strength of components by laser shot peening. *Optics and Lasers in Engg.*, 34(4-6), pp327-337.

Hibbitt, Karlsson and Sorensen, Inc. (1997). ABAQUS theory manual.

Hill R (1998). *The mathematical theory of plasticity*. Oxford Engg. Sci. Series. Clarendon Press; Oxford University Press.

Huang Y (1991). A user-material subroutine incorporating single crystal plasticity in the ABAQUS finite element program. Mech. Report 178, Div. of Applied Sciences, Harvard University.

Hutchinson JW (1976). Bounds and self-consistent estimates for creep of polycrystalline materials. *Proc. of Royal Society of London A – Math. Phys. and Engg. Sciences*, 348(1652), pp101-127.

Kysar JW (1997). Addendum to a user-material subroutine incorporating single crystal plasticity in the ABAQUS finite element program. Mech. Report 178. Div. of Applied Sciences, Harvard University.

Kysar JW, CL Briant (2002). Crack tip deformation fields in ductile single crystals. *Acta Materialia*, 50(9), pp2367-2380.

Kupperman DS, KJ Reimann, J Abregolopez (1987). Ultrasonic NDE of cast stainless-steel. *NDT Int.*, 20(3), pp145-152.

Nemat-Nasser S, T Okinaka, V Nesterenko, MQ Liu (1998). Dynamic void collapse in crystals: Computational modelling and experiments. *Philosophical Magazine A – Physics of Cond. Matter Structure Defects and Mech. Properties*, 78(5), pp1151-1174.

Peirce D, RJ Asaro, A Needleman (1983). Material rate dependence and localized deformation in crystalline solids. *Acta Metall.*, 31(12), pp1951-1976.

Peyre P, A Sollier, I Chaieb, L Berthe, B Bartnicki, C Braham, R Fabbro (2003). FEM simulation of residual stresses induced by laser peening. *European Physical J. – Applied Physics*, 23(2), pp83-88.

Rice JR (1987). Tensile crack tip fields in elastic ideally plastic crystals. *Mech. of Mat.*, 6(4), 317-335.

Rose JL, K Balasubramaniam, A Tverdokhlebov (1989). A numerical integration Green's function model for ultrasonic field profiles in mildly anisotropic media. *J. of Nondestructive Eval.*, 8(3), pp165-179.

Schmid E (1931). Articles on the physics and metallography of magnesiums. *Zeitschrift Fur Elektrochemie Und Angewandte Physikalische Chemie*, 37, pp447-459.

Tverdokhlebov A, JL Rose (1988). On Green-functions for elastic-waves in anisotropic media. *J. of the Acoustical Soc. of America*, 83(1), pp118-121.

Ungar T, H Mughrabi, D Ronnpagel, M Wilkens (1984). X-ray line-broadening study of the dislocation cell structure in deformed [001]-orientated copper single-crystals. *Acta Metallurgica*, 32(3), pp333-342.

Vukelić S, Y Wang, JW Kysar, YL Yao (2008a). Comparative study of symmetric and asymmetric deformation of Al single crystal under micro scale laser shock peening. Accepted to *J. of Mech. of Mat. and Structures*.

Vukelić S, Y Wang, JW Kysar, YL Yao (2008b). Dynamic material response of aluminum single crystal under micro scale laser shock peening. Accepted to *J. of Mfg. Science and Engg.*

Wang Y, JW Kysar, YL Yao (2008). Analytical solution of anisotropic plastic deformation induced by micro-scale laser shock peening. *Mech. of Mat.*, 40(3), pp100-114.

Zhang W, YL Yao (2002). Microscale laser shock processing of metallic components. *J. of Mfg. Science and Engg.*, 124, pp369-378.